Photocatalytic Oxidation of Propylene with Molecular Oxygen over Highly Dispersed Titanium, Vanadium, and Chromium Oxides on Silica

Fumiaki Amano, Tsuyoshi Yamaguchi, and Tsunehiro Tanaka*

Department of Molecular Engineering, Graduate School of Engineering, Kyoto University, Kyoto 615-8510, Japan

Received: October 11, 2005; In Final Form: November 9, 2005

Photocatalytic oxidation of propylene with molecular oxygen at room temperature was investigated over various silica-supported metal oxides with low loading. The photocatalytic active site is assumed to be the isolated tetrahedrally coordinated metal oxides in the ligand-to-metal charge-transferred state, such as $(M^{\delta-}-O_L^{\delta+})^*$. Photocatalytic epoxidation of propylene into propylene oxide was promoted over silica-supported V and Ti oxides at steady state. Over silica-supported Cr oxide, the propylene oxide formation rate was remarkably decreased with the time course in the reaction. The oxidation state and the coordination environment of the supported Ti, V, and Cr oxide species were determined by diffuse reflectance UV−vis spectroscopy (DRS) and electron spin resonance (ESR). During the photocatalytic oxidation, the oxidation state of the Ti^{4+} species was not varied. On the other hand, the V^{5+} species was partially reduced to V^{4+} and the Cr^{6+} species was successively reduced to Cr^{5+} and Cr^{3+}. An isotopic tracer study of the $C_3H_6-{}^{18}O_2$ reaction suggests the difference of the active oxygen species between TiO_2/SiO_2 and V_2O_5/SiO_2. The active oxygen species on TiO_2/SiO_2 is derived from molecular oxygen. On the other hand, the photogenerated products on V_2O_5/SiO_2 incorporate the lattice oxygen of the surface metal oxide species. It is suggested that the kinds of terminal ligand (hydroxyl or oxo) of the tetrahedrally coordinated metal oxides on silica decide the active oxygen species in the photocatalytic oxidation. A photoinduced hole center on the monohydroxyl $(SiO)_3Ti-OH$ species activates molecular oxygen that reacts with propylene. In the case of the monooxo $(SiO)_3V=O$ and dioxo $(SiO)_2Cr=O_2$ species, the photoactivated lattice oxygen $(O_L^-)^*$ directly reacts with propylene.

Introduction

Propylene oxide is the most desirable product in the aerobic oxidation of propylene. One of the strategies for selective epoxidation of propylene is to create electrophilic oxygen species by activation of molecular oxygen in photosystems.[1] Photocatalytic epoxidation of propylene with molecular oxygen has been reported over various kinds of silica-based catalysts at room temperature.[2] For example, TiO_2/SiO_2 of low Ti content exhibits high selectivity to propylene oxide (such as 60%) under UV irradiation,[3−5] in contrast to the deep oxidation over TiO_2 semiconductor photocatalyst.[6] The active oxygen species for photocatalytic epoxidation over TiO_2/SiO_2 is revealed to be O_3^- species, which is generated from the reaction between an O_2 molecule and a photoformed hole center (O_L^-) on the lattice oxygen of the highly dispersed titanium oxide species.[4,5] In the electrophilic O_3^- species, the electron density of the molecular oxygen unit would be decreased by electron donation to the photogenerated hole on the lattice oxygen $(O_2^{\bullet+}\cdots O_L^{2-})$.

H. Yoshida has summarized the roles of silica materials for the photocatalytic system of the highly dispersed metal oxides as follows: (1) extensive dispersion of metal oxides in the isolated tetrahedral state; (2) localization of the charge-transferred excitation on the isolated metal oxide species due to the electric nonconductance of silica; (3) decrease of side reaction since the bare silica surface is basically inert for catalytic reaction; and (4) transparency for UV and visible light.[7] It has become generally accepted that the isolated tetrahedrally coordinated MO_4 species are necessary for the high selectivity to photocatalytic epoxidation. However, the isolated tetrahedral VO_4 species on silica was considered to be inefficient for photocatalytic epoxidation. In the case of $C_3H_6-O_2$ reaction over V_2O_5/SiO_2, which promotes photocatalytic partial oxidation of light alkenes into corresponding aldehydes and ketones, propylene oxide was not detected as gaseous product.[8]

Recently, we adopted a flow reactor system for photocatalytic oxidation in place of a conventional closed reactor system.[9] The short contact time in the flow reactor reduced the isomerization and the resultant decomposition of the photooxygenated intermediates. Steady-state propylene oxide formation was promoted even over highly loaded V_2O_5/SiO_2. High selectivity into propylene oxide formation (such as 40%) is achieved at very low loading of less than 0.02 V/nm^2.

The photooxidation mechanism over V_2O_5/SiO_2 is considered to involve the insertion step of photoexcited lattice oxygen (electrophilic O_L^-) into hydrocarbons.[8] On the other hand, it has been reported that photocatalytic epoxidation was promoted by photoformed O_3^- species and the inserted oxygen was derived from molecular oxygen over TiO_2/SiO_2.[4,5] It is unresolved which active oxygen species is for the photocatalytic epoxidation over V_2O_5/SiO_2—the photoactivated lattice oxygen or the electrophilic molecular oxygen unit in O_3^- species—because the reaction mechanism of such low loaded V_2O_5/SiO_2 has not been investigated.

The oxidation state and the local structure of the metal oxide species during photooxidation were examined by means of UV−vis diffuse reflectance spectroscopy (DRS) and electron para-

* Corresponding author. E-mail: tanakat@moleng.kyoto-u.ac.jp. Telephone: (+81) 75 383 2558. Fax: (+81) 75 383 2561.

10.1021/jp0557868 CCC: $33.50
Published on Web 12/14/2005

TABLE 1: Results of Photooxidation of Propylene with Molecular Oxygen at 303 K[a]

sample	M/(M + Si) (mol %)	C_3H_6 conv rate/ μmol h^{-1}	PO yield/ μmol h^{-1}	selectivity (%) PO	propanal (C_2H_5CHO)	acetone (CH_3COCH_3)	propenal (C_2H_3CHO)	ethanal (CH_3CHO)	CO_2
TiO_2/SiO_2	0.1	35.9	17.9	50	1	9	2	18	21
V_2O_5/SiO_2	0.1	68.9	25.5	37	2	8	6	37	10
	0.3	39.1	12.2	31	2	6	7	41	13
Nb_2O_5/SiO_2	0.1	31.0	12.3	40	3	15	3	20	20
CrO_3/SiO_2	0.1	3.3	1.4	42	n.d.	11	4	21	21
ZnO/SiO_2	0.1	2.5	1.6	62	n.d.	n.d.	n.d.	7	31
MgO/SiO_2	1.5	1.8	1.3	74	n.d.	n.d.	n.d.	trace	27
SiO_2		1.9	1.4	73	n.d.	n.d.	n.d.	trace	27
Na−Y		11.0	0.6	5	n.d.	n.d.	n.d.	trace	91
TiO_2/HMS	0.1	32.4	17.4	53	0	6	5	17	18
TiO_2/FSM-16	0.1	19.2	6.6	35	4	6	4	27	24
V_2O_5/HMS	0.1	61.9	23.2	37	2	9	4	37	11
V_2O_5/FSM-16	0.1	48.8	3.8	8	5	18	4	40	26

[a] The data were obtained at 300 min on stream.

magnetic resonance (EPR). An isotopic tracer measurement using the $C_3H_6-{}^{18}O_2$ reaction was performed to compare the photocatalytic oxygen species over loaded V_2O_5/SiO_2 and TiO_2/SiO_2. These approaches provide us new insight into the relationship between the local structures of the photocatalytic active sites and the nature of the photocatalytic oxygen species.

Experimental Section

Catalyst Preparation. Amorphous silica was prepared by the hydrolysis of tetraethyl orthosilicate (TEOS) in a water−ethanol mixture at the boiling point, followed by calcination in dry air at 773 K for 5 h. Mesoporous silica with long-range hexagonal structure, FSM-16, was prepared from water glass as the silicon source using cetyltrimethylammmonium bromide ($[C_{16}H_{33}N(CH_3)_3]Br$) as a template, and the procedure was previously reported in detail.[10] Mesoporous silica with wormhole structures, HMS, was prepared from TEOS as the silicon source using dodecylamine (DDA; $CH_3(CH_2)_{11}NH_2$) as a template according to the literature procedure.[11,12] The synthesis was carried out by dissolving 1.4 g of DDA into ethanol and diluting the solution with 18 mL of water. A 5.2 g sample of TEOS was added to the solution under vigorous stirring. The reaction solution (molar composition of which was 1 TEOS:0.3 DDA: 40 H_2O:6 ethanol) was stirred at ambient temperature for 20 h. The resulting gel was filtered, washed with water, dried at 353 K, and subsequently calcined in dry air at 873 K for 5 h.

The X-ray diffraction pattern and the nitrogen adsorption isotherm at 77 K for the prepared HMS were similar to those previously reported. The BET specific surface areas of amorphous silica, FSM-16, and HMS were 650, 1060, and 1020 $m^2 g^{-1}$, respectively.

Silica-supported metal oxide catalysts were prepared by impregnation of 3.0 g of silica with a 100 mL aqueous solution dissolving the necessary amount of metal precursors at 353 K for 2 h, followed by evaporation to dryness. The precursors to supported metal oxides were $(NH_4)_2TiO(C_2O_4)_2 \cdot 2H_2O$, NH_4VO_3, $NH_4[NbO(C_2O_4)_2(H_2O)_2]$, $Cr(NO_3)_3 \cdot 9H_2O$, $(CH_3COO)_2Zn \cdot 2H_2O$, and $Mg(NO_3)_3 \cdot 6H_2O$. The loading amount of metal ions in samples was adjusted to be 0.1 mol % [M/(M + Si)] except for MgO/SiO_2 (1.5 mol %). All the samples were air-dried at 353 K and subsequently calcined in dry air at 773 K for 5 h.

Photocatalytic Reactions. Photooxidation of propylene was carried out under a gas mixture of 20% C_3H_6/10% O_2/70% He at a total flow rate of 100 mL min^{-1} at atmospheric pressure around room temperature. About 300 mg of catalyst (particulate size 26−50 mesh) was packed in a flow cell (volume 0.75 mL, irradiated area 7.5 cm^2) made of quartz glass and heated at 673 K under a He-balanced 20% O_2 stream at a flow rate of 50 mL min^{-1} for 2 h prior to the reaction. The light was irradiated through a water filter from a 300 W xenon arc lamp (Perkin-Elmer, CERAMAX PE300BUV) with reflection by a cold mirror that can permit UV−vis light with $240 < \lambda < 440$ nm. The temperature of the catalyst bed was around 303 K during the irradiation. The products were analyzed by gas chromatographs (a PEG 20M column with an flame ionization detector and a Shincarbon T column with a thermal conductivity detector) connected directly to the flow reactor.

Spectroscopies. UV−vis DRS spectra were obtained using a Perkin-Elmer Lambda-19 spectrometer equipped with an integrating sphere at room temperature. $BaSO_4$ was used as a standard reflection sample. The sample (particulate size 26−50 mesh) was packed in the flow cell and treated at the same conditions as the photocatalytic test.

X-band EPR spectra were recorded with a JEOL JES-SRE2X spectrometer at room temperature and 123 K. The 100 mg sample was pretreated by evacuation for 30 min and calcination with 100 Torr (1 bar = 750 Torr) of oxygen for 1 h at 673 K, and subsequently by evacuation for 30 min at the same temperature. The g factor was determined using Mn^{2+} marker included in MgO.

Fourier transform infrared (FT-IR) measurements were carried out using a Perkin-Elmer Spectrum One spectrometer in transmission mode at room temperature. Twenty-five grams of the catalyst was pressed into a self-supporting wafer and mounted in an in situ cell equipped with NaCl windows. Prior to the measurements, the wafers were evacuated for 30 min and calcined with 100 Torr of oxygen for 2 h at 673 K, followed by evacuation for 30 min at the same temperature. The data acquisitions consisted of 25 spectra with a resolution of 4 cm^{-1}.

Results

Photocatalytic Oxidation of Propylene. We reassessed the photocatalytic abilities of various kinds of highly dispersed metal oxides on silica by use of a flow reactor system. The catalysts, such as MgO/SiO_2,[13] Nb_2O_5/SiO_2,[14] CrO_3/SiO_2,[15] and ZnO/SiO_2,[16] have been reported as effective photocatalysts for propylene epoxidation in a closed reactor system. Table 1 summarizes the results of the photooxidation of propylene with molecular oxygen at 303 K. Propylene oxide as a gaseous product was detected over every silica-supported metal oxide and even over bare silica. High propylene oxide yield was achieved over V, Ti, and Nb oxides on silica. Na ion exchanged

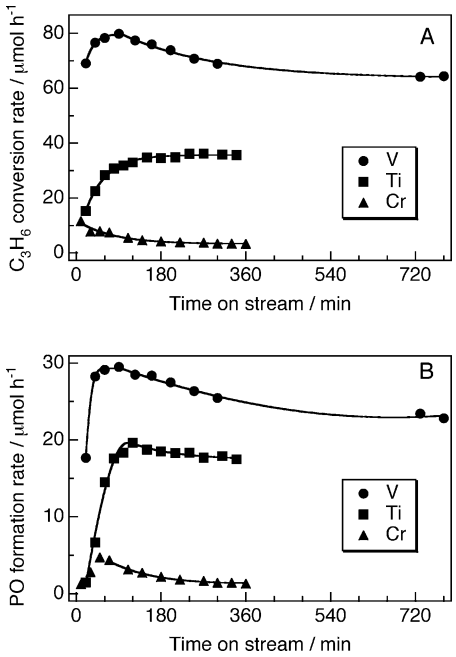

Figure 1. Time course of photooxidation of propylene in a flow reactor over 0.1 mol % V_2O_5/SiO_2 (●), TiO_2/SiO_2 (■), and CrO_3/SiO_2 (▲): conversion rate of propylene (A) and formation rate of propylene oxide (B).

Y zeolite was not effective for the present conditions, which can promote photooxidation of propylene to allyl allchols by the large electrostatic field stabilizing charge-transferred propylene$^{\bullet+}$−$O_2^{\bullet-}$ pair.[17,18] Among the silica materials, amorphous silica and HMS were more effective than FSM-16 for supported TiO_2 and V_2O_5 photocatalysts. When FSM-16 was used for support material, the production ability of propylene oxide was significantly diminished. This is probably because FSM-16 silica has acid properties.[10]

Figure 1 shows the time-dependent behavior of the photocatalytic oxidation of propylene over V_2O_5/SiO_2, TiO_2/SiO_2, and CrO_3/SiO_2 under irradiation at 303 K. The conversion rate of propylene and the formation rate of propylene oxide were increased in the order Cr < Ti < V oxides on silica. In the case of TiO_2/SiO_2, the initial activity was increased and reached the steady state at time greater than 180 min. Because this catalyst shows considerable activity at the initial period in the previously reported closed reactor system,[4] the induction period is not only due to an activation of the catalyst but is also due to a delay of the desorption of the photogenerated products from the catalyst surface. By contrast, gradual deactivation was observed for CrO_3/SiO_2 with the course of the photoreaction, although the initial activity was almost same as that of TiO_2/SiO_2.

UV−Vis Diffuse Reflectance Spectroscopy (DRS) of Supported Ti, V, and Cr Oxides. DRS spectra of supported Ti, V, and Cr oxides are characterized by transitions of the types ligand-to-metal charge transfer (LMCT) and d−d charge transfer. It is clear that the band maxima of the LMCT transitions of supported metal oxides shift to lower energy (higher nanometers) with increasing coordination number and degree of polymerization.[19,20] Figures 2, 3, and 4 show the DRS spectra of TiO_2/SiO_2, V_2O_5/SiO_2, and CrO_3/SiO_2 catalysts, respectively. No absorption was observed on bare amorphous silica.

Figure 2 shows the DRS spectra of the TiO_2/SiO_2 catalyst before and after the photooxidation of propylene with molecular oxygen. Freshly calcined sample exhibited a large absorption band centered at 210 nm (47 620 cm^{-1}) and a weak shoulder at

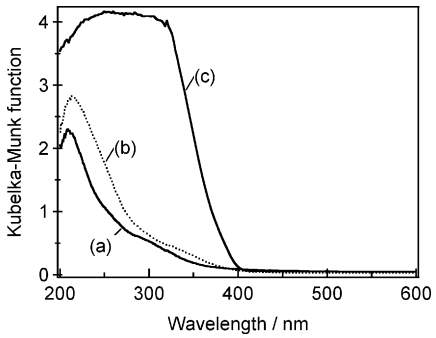

Figure 2. Diffuse reflectance UV−vis spectra of 0.1 mol % TiO_2/SiO_2 after treatment with (a) calcination at 673 K, (b) irradiation in a flow of 20% C_3H_6/10% O_2/He for 5 h at 303 K, and (c) TiO_2 (JRC-TIO-4, predominantly anatase).

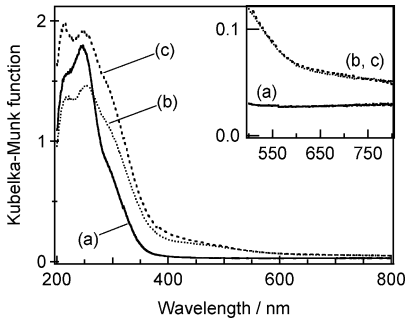

Figure 3. Diffuse reflectance UV−vis spectra of 0.1 mol % V_2O_5/SiO_2 after treatment with (a) calcination at 673 K, (b) irradiation in a flow of 20% C_3H_6/10% O_2/He for 5 h at 303 K, and (c) irradiation in a flow of 5% H_2/He at room temperature.

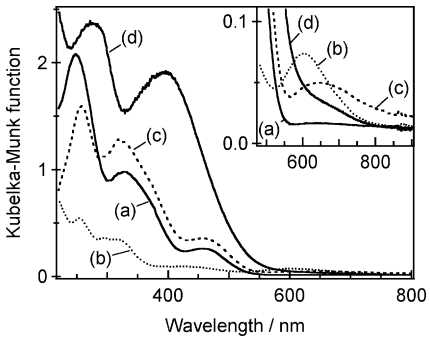

Figure 4. Diffuse reflectance UV−vis spectra of 0.1 mol % CrO_3/SiO_2 after treatment with (a) calcination at 673 K, (b) irradiation in a flow of 20% C_3H_6/10% O_2/He for 5 h at 303 K, (c) following oxidation of sample b in a flow of 20% O_2/He for 1 h at 673 K, and (d) CrO_3 diluted with $BaSO_4$.

300 nm (33 330 cm^{-1}). The narrow band at ca. 210 nm is assigned to the LMCT transition (from O_L^{2-} to Ti^{4+}) of isolated tetrahedral TiO_4 species.[20] The presence of a weak shoulder around 300 nm suggests that TiO_2/SiO_2 contains a small amount of polymerized titanium oxide species. Since the shoulder is around 300 nm, the size of the polymerized titanium oxide species is smaller than that of TiO_2 crystallite from polymerized TiO_6 octahedra, which shows a larger LMCT band below the band gap of ca. 400 nm (25 000 cm^{-1}) in Figure 2c. The DRS spectrum of the sample quenched in the photoreaction with C_3H_6 and O_2 was hardly changed from that of the freshly calcined sample. No band around the region of d−d transition indicates the absence of Ti^{3+}.

Figure 3 shows DRS spectra of the V_2O_5/SiO_2 catalysts before and after the photooxidation of propylene. Freshly calcined sample exhibited a large absorption band centered at 250 nm

(40 000 cm^{-1}) and a weak shoulder at 310 nm (32 260 cm^{-1}). These bands are assigned to LMCT transitions of isolated tetrahedrally coordinated V^{5+} oxides on silica.[19] The local structure of the surface vanadium oxides on silica is strongly affected by a water adsorption, which causes a red shift of the LMCT absorption edge. At the hydrated state, the 0.1 mol % V_2O_5/SiO_2 catalysts exhibit two LMCT bands with maxima at 245 nm (40 820 cm^{-1}) and 360 nm (27 780 cm^{-1}). The band centered at 360 nm is attributed to polymerized vanadium oxides, since the absorption edge energy (20 000 cm^{-1}) is lower than that of NH_4VO_3 crystallites (25 000 cm^{-1}; metavanadate chains from tetrahedral VO_4 polymers) and higher than that of V_2O_5 crystallites (17 540 cm^{-1}; square-pyramidal VO_5 polymers or highly distorted octahedral VO_6 polymers). The photoreaction with C_3H_6 and O_2 resulted in a shift of the absorption edge to higher nanometers and a growth of a broad band around 400−600 nm. The sample irradiated with 5% H_2 stream also showed these bands at the same positions as the sample irradiated with propylene and oxygen. The presence of V^{4+} is characterized by a weak absorption band due to d−d transition centered at 770 nm (12 900 cm^{-1}). Both photoreacted samples exhibited a very weak absorption around 650−800 nm (15 380−12 500 cm^{-1}) as shown in the inset of Figure 3, which is probably assigned to the d−d transition of V^{4+}.

Figure 4 shows DRS spectra of CrO_3/SiO_2 catalysts before and after the photooxidation of propylene. Freshly calcined CrO_3/SiO_2 showed three absorption bands centered at 245, 325, and 460 nm (40 820, 30 770, and 21 740 cm^{-1}) due to the charge transfers from O_L^{2-} to Cr^{6+} of the chromate species. The spectrum is in good agreement with the previously reported spectrum for the isolated CrO_4 tetrahedra incorporated in HMS.[21] A CrO_3 crystallite from $Cr^{6+}(d^0)$ in tetrahedral symmetry shows two LMCT bands centered at 276 and 396 nm (36 230 and 25 250 cm^{-1}) and a weak additional band in the 580−800 nm (12 500−17 240 cm^{-1}) region that is assigned to the d−d transitions of octahedral $Cr^{3+}(d^3)$ (Figure 4d). A Cr_2O_3 crystallite consisting of Cr^{3+} in octahedral symmetry showed a large d−d transition band centered at 600 nm (16 670 cm^{-1}). In the calcined catalyst, there was no band in the d−d transition region, indicating that the oxidation state is Cr^{6+} and the chromium species is in a highly dispersed tetrahedral form. Weckhuysen et al. reported that isolated and dimerized tetrahedral species existed over 0.2 wt % Cr/SiO_2, and additional polychromate species and Cr_2O_3 clusters are formed with an increase of Cr loading.[22] The photoreaction with C_3H_6 and O_2 immediately changed the yellow color of the freshly calcined catalyst to white due to the decrease of the LMCT absorption around the visible region. The sample quenched after the photoreaction shows a weak band due to d−d transitions centered at 605 nm (16 530 cm^{-1}). This indicates that Cr^{6+} on silica was photoreduced to a lower oxidation state such as Cr^{3+}. Reoxidation with 20% O_2 stream at 673 K recovered the three absorption bands of the LMCT transition. However, the d−d transition band had not fully disappeared and the band maximum was shifted to higher wavelength. It was difficult to oxidize the photoreduced chromate species with molecular oxygen even at 673 K. Therefore, the remarkable deactivation of CrO_3/SiO_2 in the time course would be correlated to the reduction of the photoactive Cr^{6+} species to inactive Cr^{3+} species.

Electron Paramagnetic Resonance (EPR) of Supported Ti, V, Cr Oxides. Figures 5, 6, and 7 show the EPR spectra of TiO_2/SiO_2, V_2O_5/SiO_2, and CrO_3/SiO_2 catalysts, respectively. In these measurements, the samples were calcined at 673 K and treated in a batch reactor connected to a vacuum line. The treated sample was transferred to a quartz tube in vacuo and sealed without exposure to the air.

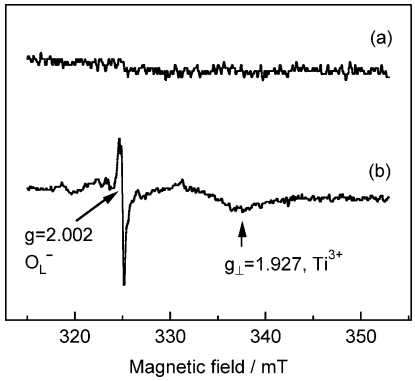

Figure 5. EPR spectra at room temperature of 0.1 mol % TiO_2/SiO_2 after calcination and outgassing at 673 K (a) and irradiation in the presence of 20 Torr of C_3H_6 and 10 Torr of O_2 for 150 min at room temperature and outgassing (b).

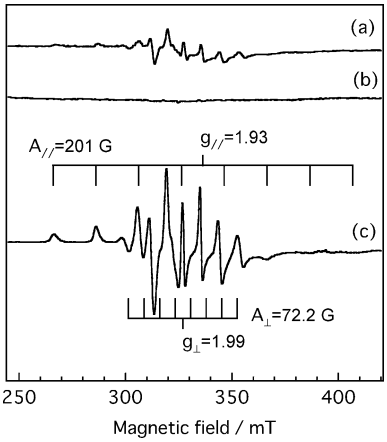

Figure 6. EPR spectra at room temperature of 0.1 mol % V_2O_5/SiO_2 after outgassing at room temperature (a), calcination and outgassing at 673 K (b), and irradiation in the presence of 20 Torr of C_3H_6 and 10 Torr of O_2 for 30 min at room temperature and outgassing (c).

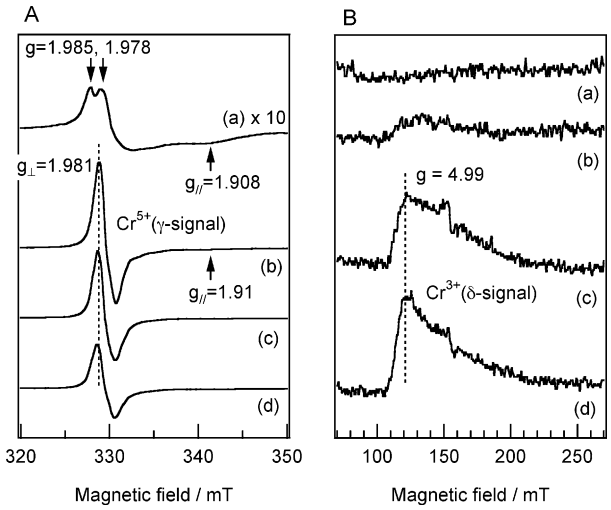

Figure 7. EPR spectra of 0.1 mol % CrO_3/SiO_2 at room temperature (A) and 123 K (B). The spectra were recorded after calcination and outgassing at 673 K (a), irradiation in the presence of 20 Torr of C_3H_6 and 10 Torr of O_2 for 1 min (b), 10 min (c), and 30 min (d) at room temperature and outgassing.

No EPR signal was observed over the freshly calcined TiO_2/SiO_2 in the dark at room temperature and 77 K. Under irradiation, radiation-induced hole centers on lattice oxygen

(O_L^-) and $Ti^{3+}(d^1)$ were observed due to the LMCT transition from O_L^{2-} to Ti^{4+}.[4] When the sample was irradiated in the presence of 20 Torr of C_3H_6 and 10 Torr of O_2 for 150 min, an EPR signal assigned to O_L^- ($g = 2.002$) and a very tiny and broad signal with axial symmetric $\boldsymbol{g}$ tensor due to Ti^{3+} ($g_\perp = 1.93$) was also detected at room temperature (Figure 5b). Though the signal of the parallel component was not obviously determined, a larger $g_\parallel$ than $g_\perp$ proves the presence of Ti^{3+} in tetragonally compressed tetrahedral symmetry.[23,24] The fraction of the charge-transferred Ti^{3+} signal is assumed to be small compared to the total amount of Ti because of the very low EPR signal intensity and the absence of the d−d transition in the DRS spectrum of TiO_2/SiO_2 irradiated with C_3H_6 and O_2 (Figure 2).

Figure 6 shows EPR spectra of V_2O_5/SiO_2 catalyst at room temperature. In the case of hydrated catalyst, which was outgassed at room temperature for 2 h, broad signals due to $V^{4+}(d^1)$ located in octahedral symmetry were observed. On the other hand, there was no EPR signal in the dehydrated sample calcined at 673 K. It is known that, in the dehydrated condition, the surface vanadium oxide species on silica are in a highly dispersed form in contrast to the polymerized form in the hydrated state. After irradiation with 20 Torr of C_3H_6 and 10 Torr of O_2, the axial symmetric EPR signal with eight hyperfine splitting due to $V^{4+}(d^1$; nuclear spin $I = 7/2$) was clearly observed ($g_\perp = 1.99$, $g_\parallel = 1.93$, $A_\perp = 72.2$ G, and $A_\parallel = 201$ G). The $\boldsymbol{g}$ and $\boldsymbol{A}$ anisotropic tensors are consistent with VO^{2+} ions in square-pyramidal or tetragonally distorted octahedral sites.[25] There was no hole center in the EPR spectrum. During the photoreaction, a part of V^{5+} species would be reduced to the octahedrally coordinated V^{4+} oxides.

Parts A and B of Figure 7 show EPR spectra of CrO_3/SiO_2 catalyst at room temperature and 77 K, respectively. Several kinds of EPR-active chromate species have been reported in supported chromium oxides such as Cr^{5+} species (γ-signal) and two types of Cr^{3+} species (β- and δ-signals).[26] The freshly calcined sample exhibits a tiny γ-signal with axial symmetry, which has two $g_\perp$ lines suggesting the superimposition of two very close axial contributions. When the sample was irradiated with 20 Torr of C_3H_6 and 10 Torr of O_2 for 1 min, the axially symmetric γ-signal ($g_\perp = 1.981$, $g_\parallel = 1.91$) composed of a sharp $g_\perp$ line and a weak diffuse $g_\parallel$ line was immediately increased by the reduction of $Cr^{6+}(d^0)$ to $Cr^{5+}(d^1)$. The γ-signal was gradually decreased with the irradiation time. Although any other signal was observed at room temperature, a broad δ-signal assigned to Cr^{3+} was detected at 123 K as shown in Figure 7B. There was no β-signal generally assigned to Cr_2O_3-like clusters. The broad δ-signal characterized by a positive lobe around $g = 4.4-5.0$ is assigned to isolated Cr^{3+} species.[26] The increase of the δ-signal with irradiation time indicates the following reduction of the Cr^{5+} species to the isolated Cr^{3+} species during the irradiation in the presence of C_3H_6 and O_2.

Tracer Measurement in $C_3H_6-{}^{18}O_2$ Reaction over TiO_2/SiO_2. The $C_3H_6-O_2$ reaction over TiO_2/SiO_2 in a closed reaction system was monitored by means of FT-IR spectroscopy. Figure 8A shows the difference spectra before and after the photooxidation of propylene with molecular oxygen; i.e., the spectrum recorded before irradiation was subtracted from the spectrum recorded following irradiation. The difference spectra show negative features due to the loss of propylene at 1641 and 1455 cm^{-1} assigned to C═C stretching and C−H deformational absorption, respectively. The most intense positive features were observed at 1715 cm^{-1} in C═O stretching region, and 1493 and 1409 cm^{-1} in the C−H deformational region due to the formation of the photogenerated products. The bands at 1409 and 1493 cm^{-1} are consistent with the bands observed for an authentic spectrum of propylene oxide on bare silica, which are assigned to $\delta(CH_2)$ of the epoxy group.[27] The large and broad C═O stretching band centered at 1715 cm^{-1} with a shoulder around 1685 cm^{-1} is superimposed by the bands of ethanal (1721 cm^{-1}) and acetone (1697 cm^{-1}). The broad bands due to ethanal and acetone were also confirmed in the C−H deformational region. The distributions of the photogenerated products were almost same as the result in the flow reactor system at steady state.

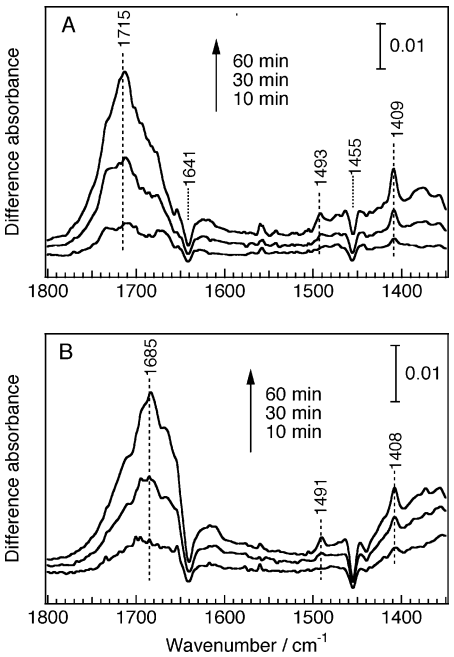

Figure 8. FT−IR difference spectra before and after irradiation of 0.1 mol % TiO_2/SiO_2 in the presence of 20 Torr of C_3H_6 and 10 Torr of $^{16}O_2$ (A) and $^{18}O_2$ (B) for 10, 30, and 60 min.

Figure 8B shows the difference spectra of the $C_3H_6-{}^{18}O_2$ reaction over TiO_2/SiO_2. When ^{18}O-labeled molecular oxygen was used, the absorption due to the C═^{16}O stretching (1715 cm^{-1}) was hardly detected but the corresponding labeled C═^{18}O stretching absorption (1685 cm^{-1}) was observed. These observations prove that the active oxygen species was derived from molecular oxygen in the photooxidation of propylene over TiO_2/SiO_2. An isotropic effect on the peak position was not clearly observed in the C−H deformational region.

Tracer Measurement in $C_3H_6-{}^{18}O_2$ Reaction over V_2O_5/SiO_2. Figure 9A shows the FT-IR difference spectra of the $C_3H_6-{}^{16}O_2$ reaction over V_2O_5/SiO_2. The C−H deformational band due to the epoxy group of propylene oxide was confirmed at 1409 cm^{-1}. The most intense positive features were observed at 1715, 1692, and 1682 cm^{-1} in the C═O stretching region. On the basis of the authentic spectra on silica, we can assign the bands centered at 1715, 1692, and 1682 cm^{-1} to ethanal, acetone, and propenal (acrolein), respectively.

Figure 9B shows the difference spectra of the $C_3H_6-{}^{18}O_2$ reaction over V_2O_5/SiO_2 in a closed reaction system. When ^{18}O-labeled molecular oxygen was used, the growth of four bands centered at 1715, 1685, 1666, and 1656 cm^{-1} was observed with irradiation time. In contrast to the result on TiO_2/SiO_2, the ^{16}O-labeled carbonyl stretching at 1715 cm^{-1} due to ethanal was clearly detected. This indicates the presence of lattice oxygen insertion in the photogenerated carbonyl compounds over V_2O_5/SiO_2. We assigned the new bands centered at 1666 and 1656 cm^{-1} to the ^{18}O-labeled carbonyl stretchings of acetone

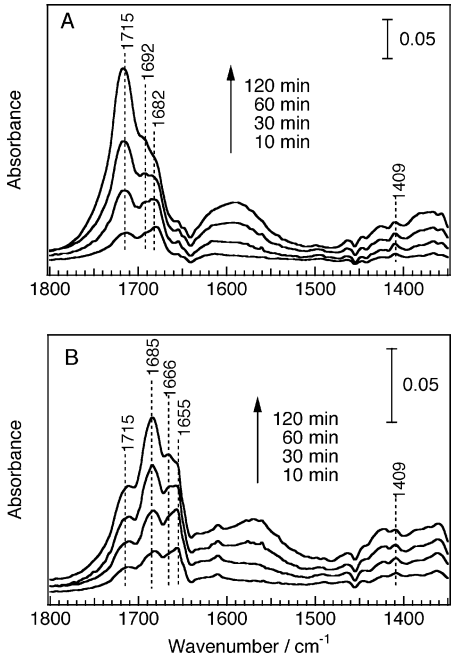

Figure 9. FT−IR difference spectra before and after irradiation of 0.3 mol % V_2O_5/SiO_2 in the presence of 20 Torr of C_3H_6 and 10 Torr of $^{16}O_2$ (A) and $^{18}O_2$ (B) for 10, 30, 60, and 120 min.

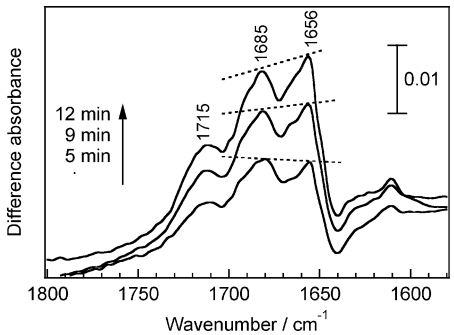

Figure 10. FT−IR difference spectra before and after irradiation of 0.3 mol % V_2O_5/SiO_2 in the presence of 20 Torr of C_3H_6 and 10 Torr of $^{18}O_2$ for 5, 9, and 12 min.

and acrolein, respectively. The band centered at 1685 cm^{-1} is superimposed by the C═^{18}O stretching of ethanal and C═^{16}O stretchings due to acetone and acrolein.

Figure 10 shows the initial evolution of the carbonyl absorption in the FT-IR difference spectra of the $C_3H_6-{}^{18}O_2$ photoreaction over V_2O_5/SiO_2. The irradiation caused the growth of approximately three bands centered at 1715, 1685, and 1656 cm^{-1}. The band at 1715 cm^{-1} is due to C═^{16}O stretching of ethanal. The band at 1685 cm^{-1} consists of the superimposition by the C═^{18}O stretching of ethanal and the C═^{16}O stretching of acrolein. The band at 1656 cm^{-1} is assignable to the C═^{18}O stretching of acrolein. With an increase of the irradiation time, the intensity of the band at 1656 cm^{-1} due to only the ^{18}O-labeled component increased more significantly than that at 1685 cm^{-1} consisting of the sum of the ^{16}O- and ^{18}O-labeled components. This indicates the gradual variance of the $^{18}O/(^{16}O + {}^{18}O)$ ratio in the photogenerated carbonyl compounds with irradiation time. At more than 5 min irradiation, the inserted ratio of ^{18}O gradually increased over V_2O_5/SiO_2 photocatalyst. The parallel decrease of the ^{16}O insertion suggests that the lattice oxygen of the surface vanadium species is consumed at the initial stage and the reduced vanadium species is reoxidized by $^{18}O_2$ in the photooxidation.

SCHEME 1: Generally Proposed Local Structures of Isolated Tetrahedrally Coordinated Metal Oxides in (a) TiO_2/SiO_2, (b) V_2O_5/SiO_2, and (c) CrO_3/SiO_2

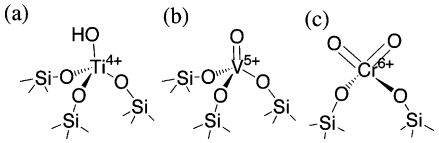

Discussion

Photocatalytic Active Sites. The local structure of highly dispersed metal oxides has been widely characterized in the heterogeneous catalysts.[19,20,28−30] In general, the dispersion of the metal oxides is dependent mainly on the loading amount in the supported catalysts, although the preparation method and the kinds of support materials are also important. When the densities of the Ti, V, and Cr oxides are low, the surface species are in the highly dispersed form with tetrahedral coordination.

Scheme 1 illustrates the generally proposed molecular structures of the isolated tetrahedral TiO_4, VO_4, and CrO_4 species on silica. The tetrahedral environments of the metal oxides have been determined by the high preedge intensity (1s−3d transitions) in the X-ray absorption near-edge structure (XANES).[19] In the case of the tetrahedrally coordinated cations, the forbidden 1s−3d transitions are partially allowed by the 3d−4p mixing due to a breakdown of the inversion symmetry. The oxo bonds have been characterized by vibrational spectroscopies and extended X-ray absorption fine structure (EXAFS). Raman bands centered at ca. 1038 and 980 cm^{-1} are attributed to the stretching vibration of oxo bonds of the isolated VO_4 and CrO_4 tetrahedra, respectively.[19,28] Curve-fitting analysis of the EXAFS also indicates the presence of two kinds of bond lengths in the oxo species on silica, a shorter bond (V═O) and three longer bonds (V−O) in the isolated VO_4 tetrahedra,[29,31] and two shorter bonds (Cr═O) and two longer bonds (Cr−O) in the isolated CrO_4 tetrahedra.[28] By contrast, an oxo bond has not been observed in the highly dispersed titanium oxide system. The EXAFS analysis of the isolated TiO_4 tetrahedra on silica shows four equivalent Ti−O bonds.[30] Maschmeyer et al. have proposed a plausible structure containing a hydroxyl and three siloxyl bonds in Ti grafted on MCM-41 silica prepared from titanocene dichloride.[32] Note that the very weak Raman and IR bands at 940−960 cm^{-1} are assigned not to an oxo bond but to Si−OH group perturbed by a nearby Ti cation.[20]

Dehydrated V_2O_5/SiO_2 shows the long-lived photoluminescence emission (millisecond order) with a vibrational fine structure.[9,33] The energy separation of the progression between 0−0 and 0−1 transitions is about 950−1050 cm^{-1}, which is generally assigned to the vibrational stretching of the terminal V═O bond of the isolated VO_4 species. The emission is attributed to a radiative decay from the charge-transferred triplet state $(V^{4+}-O_L^-)^*$ via the singlet excited sate. UV irradiation causes the charge transfer from O^{2-} to V^{5+}. The promotion from a nonbonding electron into the antibonding molecular orbital of V═O bond ($n \rightarrow \pi^*$ transition) destabilizes and activates the lattice terminal oxygen. It has been reported that CrO_3/SiO_2 also exhibits fine-structured photoluminescence emission, although the emission intensity was somewhat lower than that of V_2O_5/SiO_2.[34] The same as vanadium oxide on silica, the isolated oxide species in charge-transferred states, $(Ti^{3+}-O_L^-)^*$ and $(Cr^{5+}-O_L^-)^*$, are assumed to be photocatalytic active sites in TiO_2/SiO_2 and CrO_3/SiO_2, respectively.

Mechanism of Photocatalytic Oxidation. TiO_2/SiO_2 and V_2O_5/SiO_2 catalyzed the selective photooxidation of propylene with molecular oxygen. On the other hand, CrO_3/SiO_2 was not effective for the steady-state reaction. In the former case, since the ability of propylene oxide production was very stable, an electrophilic oxygen species would be continuously generated through the photocatalytic cycle.

DRS and EPR techniques show that the tetrahedrally coordinated Ti^{4+} in TiO_2/SiO_2 does not undergo variation of the oxidation state during irradiation with C_3H_6 and O_2. Although the charge-transferred $(Ti^{3+}-O_L^-)^*$ species was confirmed in vacuo by EPR (Figure 5), these signals disappeared in the reaction with molecular oxygen to produce $O_2^{\bullet-}$ and O_3^- ($O_2^{\bullet+}\cdots O_L^{2-}$) species.[4] In contrast, the tetrahedrally coordinated V^{5+} and Cr^{6+} oxides were reduced to the lower oxidation state during the photoreaction. If the lattice oxygen directly reacts with hydrocarbon similarly to the redox-type "Mars and van Krevelen" mechanism, the oxidation state of the metal cations will be varied during the photoreaction. Therefore, the presence of the reduced cations indicates that the photoactivated oxo species is responsible for the photocatalytic oxidation over V_2O_5/SiO_2 and CrO_3/SiO_2.

The isotopic tracer study of the $C_3H_6-{}^{18}O_2$ photoreaction also indicated the lattice oxygen insertion in the photogenerated carbonyl compounds over V_2O_5/SiO_2. The ratio of the ^{16}O insertion to ^{18}O was gradually decreased during the $C_3H_6-{}^{18}O_2$ reaction (Figure 10). This proves the redox photocatalytic mechanism, in which V^{5+} is reduced by propylene and subsequently oxidized by molecular oxygen. In the present study, we only monitored the oxygen insertion to the carbonyl compounds. Ethanal formation is seems to be promoted by the double bond fission of propylene.[8] Acrolein is probably formed via π-allyl intermediate in the photooxidation of propylene over V_2O_5/SiO_2.[8] Therefore, these byproducts (ethanal and acrolein) might also be produced through the double bond attack by the electrophilic oxygen species. Anyway, it is concluded that the lattice oxygen insertion progresses on V_2O_5/SiO_2 photocatalyst.

In contrast, the lattice oxygen of the isolated tetrahedral TiO_4 species was not incorporated in the photogenerated carbonyl compounds. By means of gas chromatography−mass spectrometry analysis, it has been already revealed that the photogenerated propylene oxide includes 100% ^{18}O-oxygen in the $C_3H_6-{}^{18}O_2$ reaction over isolated TiO_4 species in silica.[4,5]

Scheme 2 shows proposed reaction mechanisms in the photooxidation of propylene with molecular oxygen over V_2O_5/SiO_2, TiO_2/SiO_2, and CrO_3/SiO_2. Yoshida et al. have proposed the mechanism over the sol−gel synthesized TiO_2-SiO_2 for photocatalytic epoxidation, in which molecular oxygen was activated on the charge-transferred $(Ti^{3+}-O_L^-)^*$ species.[4,5] The active oxygen species for propylene oxide production is concluded to be an electrophilic O_3^- ($O_2^{\bullet+}\cdots O_L^{2-}$) species generated on the photoformed hole center.[4,5] Since the photoinduced electron in Ti^{3+} is consumed by molecular oxygen ($Ti^{3+} + O_2 \rightarrow Ti^{4+} + O_2^{\bullet-}$), the oxidation state of Ti^{4+} is actually constant in the presence of oxygen.

In the case of V_2O_5/SiO_2 (selectivity to propylene oxide, 37%), the photoactivated oxo ligand would be the active oxygen species for photocatalytic epoxidation of propylene. The lattice oxygen in the excited triplet state $(V^{4+}=O_L^-)^*$ is considered to exhibit electrophilic character, which preferably attacks the double bonds in propylene. The photoinduced electron on the vanadium cation will be accepted by molecular oxygen. The one side of molecular oxygen is used for replenishment of the terminal oxo group consumed by propylene. The other oxygen atom would be involved in the deep oxidation to carbon dioxide and the side reaction to carbonyl compounds.

SCHEME 2: Proposed Reaction Mechanisms in the Photooxidation of Propylene with Molecular Oxygen over (A) TiO_2/SiO_2, (B) V_2O_5/SiO_2, and (C) CrO_3/SiO_2[a]

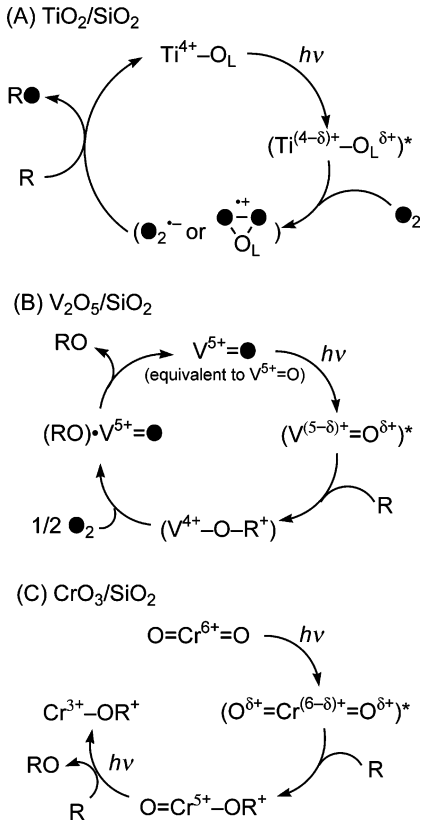

[a] R is propylene and RO is propylene oxide. The black and normal oxygen atoms are originated from molecular oxygen and lattice oxygen, respectively.

CrO_3/SiO_2 shows a quite different time course in the photooxidation of propylene with molecular oxygen, in which the activity was decreased with the time on stream. During the photoreaction, the isolated tetrahedrally coordinated Cr^{6+} species was drastically reduced to the lower oxidation state, such as Cr^{5+} and Cr^{3+}. This indicates that the deactivation of CrO_3/SiO_2 is due to the reduction of photoactive Cr^{6+} to the photoinactive species. The reduced species resisted the reoxidation by molecular oxygen even at 673 K (Figure 4). Therefore, the redox cycle of the chromate species is not promoted. Although it is reported that CrO_3/SiO_2 promotes photocatalytic oxidation of propylene and propane under visible light irradiation,[15,21] the photoreaction is stoichiometric rather than photocatalytic. Since there is initial activity, the photoactivated lattice oxygen has capability for propylene oxidation. It is concluded that the photoinduced hole centers on the lattice oxygen of the dioxo CrO_4 tetrahedron react with propylene.

Photocatalytic Site and Active Oxygen Species. There were two kinds of photocatalytic oxygen species with electrophilic character: the activated molecular oxygen ($O_2^{\bullet+}$) on the isolated TiO_4 species, and the activated lattice oxygen on the isolated VO_4 and CrO_4 species. Both types of oxygen species, which probably attack the double bond of propylene, promote epoxidation of propylene. We consider that these differences of the active oxygen species are due to the kinds of terminal oxygen ligand, such as oxo and hydroxyl ligands. In the case of the monooxo $(SiO)_3V{=}O$ and dioxo $(SiO)_2Cr{=}O_2$ species, the photoinduced hole centers on the lattice oxygens are responsible

for the activation of hydrocarbons. On the other hand, photoinduced hole centers of the hydroxyl $(SiO)_3Ti-OH$ species cause the activation of molecular oxygen, and the O_3^- species promotes the epoxidation of propylene.

Conclusion

TiO_2/SiO_2 and V_2O_5/SiO_2 promote steady-state production of propylene oxide in the photocatalytic oxidation of propylene. The photocatalytic active site is assumed to be the ligand-to-metal charge-transferred state of the isolated tetrahedrally coordinated Ti^{4+} and V^{5+} oxides on silica. By means of DRS and EPR, it was revealed that the oxidation state of the Ti^{4+} species is stable during the photoreaction with C_3H_6 and O_2, in contrast to the V^{5+} species (that is partially reduced to V^{4+}). The isotopic $C_3H_6-{}^{18}O_2$ reaction also suggests the difference of the active oxygen species between TiO_2/SiO_2 and V_2O_5/SiO_2 photocatalysts. In the case of the isolated tetrahedral TiO_4 species, molecular oxygen is activated on the photoformed hole center on the lattice oxygen. Over V_2O_5/SiO_2, the active oxygen species is the photoactivated lattice oxygen of the isolated tetrahedral VO_4 species. These differences in the photocatalytic mechanism would be dependent on the kinds of terminal ligand, such as monohydroxyl or monooxo, of the surface tetrahedrally coordinated species bound to silica surface through three bonds. In the case of monooxo VO_4 and dioxo CrO_4 species, the first step of the photooxidation starts from the reaction of photoactivated oxo ligand with hydrocarbons. On the other hand, the photoactivated monohydroxyl TiO_4 species first activates molecular oxygen rather than hydrocarbons. It is also recognized that the photooxidation activity of CrO_3/SiO_2 is decreased with time on stream due to the reduction of the oxidation state of the chromate species.

References and Notes

(1) Maldotti, A.; Molinari, A.; Amadelli, R. *Chem. Rev.* **2002**, *102*, 3811−3836.
(2) Yoshida, H.; Murata, C.; Hattori, T. *J. Catal.* **2000**, *194*, 364−372.
(3) Yoshida, H.; Murata, C.; Hattori, T. *Chem. Commun.* **1999**, 1551−1552.
(4) Murata, C.; Yoshida, H.; Kumagai, J.; Hattori, T. *J. Phys. Chem. B* **2003**, *107*, 4364−4373.
(5) Murata, C.; Hattori, T.; Yoshida, H. *J. Catal.* **2005**, *231*, 292−299.
(6) Pichat, P.; Herrmann, J. M.; Disdier, J.; Mozzanega, M. N. *J. Phys. Chem.* **1979**, *83*, 3122−3126.
(7) Yoshida, H. *Catal. Surv. Asia* **2005**, *9*, 1−9.
(8) Yoshida, S.; Tanaka, T.; Okada, M.; Funabiki, T. *J. Chem. Soc., Faraday Trans.* **1984**, *80*, 119−128.
(9) Amano, F.; Tanaka, T.; Funabiki, T. *Langmuir* **2004**, *20*, 4236−4240.
(10) Yamamoto, T.; Tanaka, T.; Funabiki, T.; Yoshida, S. *J. Phys. Chem. B* **1998**, *102*, 5830−5839.
(11) Tanev, P. T.; Chibwe, M.; Pinnavaia, T. J. *Nature* **1994**, *368*, 321−323.
(12) Pauly, T. R.; Liu, Y.; Pinnavaia, T. J.; Billinge, S. J. L.; Rieker, T. P. *J. Am. Chem. Soc.* **1999**, *121*, 8835−8842.
(13) Yoshida, H.; Tanaka, T.; Yamamoto, M.; Funabiki, T.; Yoshida, S. *Chem. Commun.* **1996**, 2125−2126. Yoshida, H.; Tanaka, T.; Yamamoto, M.; Yoshida, T.; Funabiki, T.; Yoshida, S. *J. Catal.* **1997**, *171*, 351−357.
(14) Tanaka, T.; Nojima, H.; Yoshida, H.; Nakagawa, H.; Funabiki, T.; Yoshida, S. *Catal. Today* **1993**, *16*, 297−307.
(15) Murata, C.; Yoshida, H.; Hattori, T. *Chem. Commun.* **2001**, 2412−2413.
(16) Yoshida, H.; Murata, C.; Hattori, T. *Chem. Lett.* **1999**, 901−902. Yoshida, H.; Shimizu, T.; Murata, C.; Hattori, T. *J. Catal.* **2003**, *220*, 226−232.
(17) Blatter, F.; Sun, H.; Frei, H. *Catal. Lett.* **1995**, *35*, 1−12.
(18) Xiang, Y.; Larsen, S. C.; Grassian, V. H. *J. Am. Chem. Soc.* **1999**, *121*, 5063−5072.
(19) Gao, X. T.; Bare, S. R.; Weckhuysen, B. M.; Wachs, I. E. *J. Phys. Chem. B* **1998**, *102*, 10842−10852.
(20) Gao, X. T.; Bare, S. R.; Fierro, J. L. G.; Banares, M. A.; Wachs, I. E. *J. Phys. Chem. B* **1998**, *102*, 5653−5666.
(21) Yamashita, H.; Anpo, M. *Curr. Opin. Solid State Mater. Sci.* **2003**, *7*, 471−481.
(22) Weckhuysen, B. M.; Schoonheydt, R. A.; Jehng, J. M.; Wachs, I. E.; Cho, S. J.; Ryoo, R.; Kijlstra, S.; Poels, E. *J. Chem. Soc., Faraday Trans.* **1995**, *91*, 3245−3253.
(23) Tuel, A.; Diab, J.; Gelin, P.; Dufaux, M.; Dutel, J. F.; Bentaarit, Y. *J. Mol. Catal.* **1990**, *63*, 95−102.
(24) Prakash, A. M.; Sung-Suh, H. M.; Kevan, L. *J. Phys. Chem. B* **1998**, *102*, 857−864.
(25) Davidson, A.; Che, M. *J. Phys. Chem.* **1992**, *96*, 9909−9915.
(26) Weckhuysen, B. M.; Schoonheydt, R. A.; Mabbs, F. E.; Collison, D. *J. Chem. Soc., Faraday Trans.* **1996**, *92*, 2431−2436.
(27) Lowe, M. A.; Alper, J. S.; Kawiecki, R.; Stephens, P. J. *J. Phys. Chem.* **1986**, *90*, 41−50.
(28) Wang, Y.; Ohishi, Y.; Shishido, T.; Zhang, Q. H.; Yang, W.; Guo, Q.; Wan, H. L.; Takehira, K. *J. Catal.* **2003**, *220*, 347−357.
(29) Yoshida, S.; Tanaka, T.; Nishimura, Y.; Mizutani, H.; Funabiki, T. *Proceedings of the International Congress on Catalysis, 9th*; Chemical Institute of Canada: Ottawa, 1988; Vol. 3, pp 1473−1480.
(30) Tanaka, T.; Teramura, K.; Yamamoto, T.; Takenaka, S.; Yoshida, S.; Funabiki, T. *J. Photochem. Photobiol., A* **2002**, *148*, 277−281.
(31) Amano, F.; Tanaka, T. *Catal. Commun.* **2005**, *6*, 269−273.
(32) Maschmeyer, T.; Rey, F.; Sankar, G.; Thomas, J. M. *Nature* **1995**, *378*, 159−162.
(33) Gritscov, A. M.; Shvets, V. A.; Kazansky, V. B. *Chem. Phys. Lett.* **1975**, *35*, 511−512.
(34) Hazenkamp, M. F.; Blasse, G. *J. Phys. Chem.* **1992**, *96*, 3442−3446.